Brodogradnja Volume 75, Number 3 (2024) 75306

journal homepage: www.brodogradnja.fsb.hr

Brodogradnja

An International Journal of Naval Architecture and Ocean Engineering for Research and Development

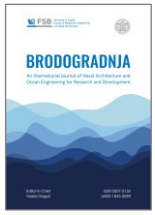

Four-quadrant propeller hydrodynamic performance mapping for improving ship motion predictions

Taner Cosgun[1*], *Mahmutcan Esenkalan*[1], *Omer Kemal Kinaci* [2,3,4]

[1] *Faculty of Naval Architecture and Maritime, Yildiz Technical University, Turkiye*
[2] *Faculty of Naval Architecture and Ocean Engineering, Istanbul Technical University, Turkiye*
[3] *Marine Cybernetics Advanced Vehicle Technologies (MARNETICS), ITU Ariteknokent, Turkiye*
[4] *Marine Robotics Laboratory, Istanbul Technical University, Turkiye*

ARTICLE INFO

Editor-in-Chief: Prof. Nastia Degiuli
Associate Editor: PhD Ivana Martić

Keywords:
Free-running ship
Ship motions
Four-quadrant propeller performance
Self-propulsion
Ship maneuvering

ABSTRACT

On the path toward fully autonomous sea vessels, forecasting a ship's exact velocity and position during its route plays a crucial role in dynamic positioning, target tracking, and autopilot operations of the unmanned body navigating toward predetermined locations. This paper addresses the prediction of the operational performance of a free-running submarine advancing in a straight route (in surge motion). Along with the forward advancing vessel (straight-ahead motion) the study covers all possible scenarios of ship's surge, including crash-ahead, crash-back, and astern motions. Conventional maneuvering models cannot handle motions other than forward advancement due to the absence of propeller data in all four quadrants of hydrodynamic performance map. This study proposes an approach for predicting submarine performance in all these surge conditions by utilizing four-quadrant propeller performance and resistance test data. We developed an in-house code, SMot4QP, to simulate ship speed and position in the time domain. We obtained satisfying results for the straight-ahead and crash-ahead motions, while the crash-back and astern maneuvers require further refinement due to propeller wake interaction with the hull. The proposed method is capable of predicting the motions of all types of vessels using the ship's resistance and four-quadrant propeller test results. Thus, SMot4QP offers a fast and robust alternative to computationally expensive free-running self-propulsion simulations for operational performance prediction in broader naval applications.

1. Introduction

The assessment of powering, propulsion and motion characteristics stands as a key topic in marine hydrodynamics due to its critical role in the preliminary design of both surface and submersible vessels. The computation of the surrounding flow field around a ship traveling at a specific velocity, by means of its own propulsive force, so-called self-propulsion, represents a preeminent technique to determine the ship's propulsion performance. In conjunction with fundamental empirical relations and experimental measurements, computational strategies are gaining increasing attention as a means to comprehensively

* Corresponding author.
E-mail address: tcosgun@yildiz.edu.tr

http://dx.doi.org/10.21278/brod75306
Submitted 02 April 2024; Accepted 05 July 2024
ISSN 0007-215X; eISSN 1845-5859

evaluate the hydrodynamic performance of self-propelled marine vehicles. As a well-established, cost & time-effective and reliable tool, computational fluid dynamics (CFD) plays a leading role in the self-propulsion estimations of ships. Especially in the last decade, CFD has been increasingly applied to various self-propulsion problems in marine hydrodynamics. Illustrating this trend, a recent study by Chase and Carrica [1] employed CFD to assess the wake behavior of a generic submarine propeller on the self-propulsion of the DARPA Sub-Off. They have examined the effectiveness of different turbulence modelling approaches along with the propulsive performance at the self-propulsion point. The self-propulsion and resistance characteristics of different submarine forms in both fully submerged and near-free surface conditions are investigated in Zhang and Zhang [2], Cosgun [3] and Dogrul [4]. Gaggero et al. [5] proposed a coupled RANS/BEM approach to reduce the computational demand of self-propulsion simulations. Jasak et al. [6] developed an extended version of an open-source CFD tool for the purpose of calculating self-propulsion performance of full-scale ships. They found the methodology quite accurate by comparing the predictions with sea trials of two different ships. Mikulec and Piehl [7] presented the sea trial data for the purpose of validation and verification of their full-scale unsteady RANS CFD simulations. Saydam et al. [8] performed ship-scale self-propulsion analyses with an oil tanker and validated the predictions with sea trial data. Oltmann and Sharma [9] proposed a mathematical model to investigate the motions of a free running single-screw tanker and a twin-screw center-rudder container carrier. They reported that their model can simulate the cases with initial forward speed changes and also can be applied even to maneuvers involving speed reversal. Dai et al. [10] conducted self-propulsion simulations in calm water and waves with varying loads to examine the propulsion performance. CFD analyses of the self-propelled Japanese Bulk Carrier was applied by Grlj et al.[11] to examine the scale effect on the propulsion characteristics. As well as the self- propulsion and other propulsive performance investigations of model or full-scale ships, CFD was applied to many other problems such as manoeuvrability [12], [13], course keeping [14], [15].

There are different mathematical models for simulations depending on the ship's type and required motions. These can range from being as broad as having all six degrees-of-freedom (DOF) to specific motions such as ship propulsion, which may only involve one single ship motion (surge). For instance, Carrica et al. [16] utilized a four-degrees-of-freedom model (neglected sway and yaw) and presented an alternative computational methodology based on a PI speed controller to achieve the target velocity in self-propulsion computations. A ship's self-propulsion computations start from the analysis of ship resistance and open-water propeller performance [17], [18]. This may also be called as the straight-ahead case, and it only considers the forward motion of the ship with the propeller's rotation. As an example for this case, Kinaci et al. [19] performed CFD calculations to investigate the self-propulsion performance of three different ships. In a study by the same group, [20] established a practical computational methodology to estimate ship self-propulsion parameters. Delen et al. [21] presented a fast and reliable methodology to estimate the propulsion performance of full-scale ships based on Telfer's GEOSIM approach. All these studies considered propeller rotation to be in a single direction when the ship is moving forward. Additionally, the last two papers presented practical ways to speed up forward-going ship self-propulsion computations. However, the surge motion also involves crash-ahead, crash-back, and astern motions, which are depicted in Figure 1. These motions depend on the ship's direction as well as the propeller's direction of rotation. In addition to serving as standard maneuvers in routine ship operations, these motions are imperative for both manned and unmanned vessels in achieving precise target positions. To control a maritime vehicle autonomously/semi-autonomously, we need to be able to calculate its movement in different scenarios quickly and in real-time. Approaches with very high computation times like free-running CFD, no matter how accurate, cannot meet this need. Therefore, there is a need for sufficiently accurate models that can also be calculated in real-time.

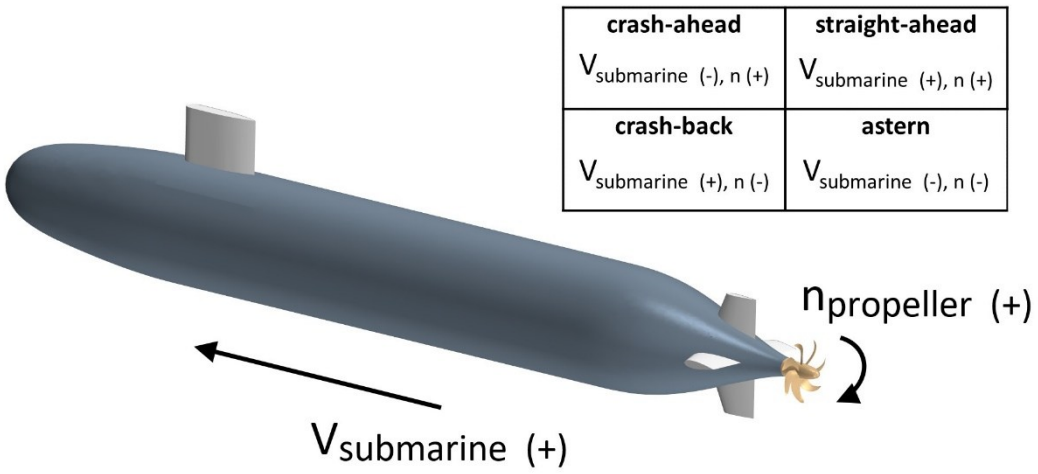

Fig. 1 Description of different surge motions

The surge motion of the ship is essentially a ship propulsion problem and is based on the balance between the resistance experienced by the hull and the thrust generated by the propeller. Ship resistance experiments only consider the forward motion and measure the force acting on the hull at different speeds. On the other hand, the open-water propeller tests allow to find a propeller's thrust and torque at different advance ratios, either in positive or negative rotation. Even traditional ship propulsion primarily concentrates on the forward direction with regular propeller rotation, the ship may also move astern, and the propeller can operate in reverse, leading to four distinct possibilities of propulsion modes. Thus, the forces acting on the ship for ahead & reversed conditions and open-water propeller performance data for regular and reversed rotations are needs to be considered for the accurate prediction models for straight-ahead, crash-ahead, crash-back, and astern ship motions.

As stated, traditional ship motion simulations only include the forward motion of the ship and the models used for this purpose are generally insufficient when the propeller is working reversed and/or the ship is moving astern. Since maneuvering models only incorporate propeller thrust within the first quadrant, they make mathematical models of dynamic positioning systems inadequate for holistic simulations. The goal in this study is to develop a basis for enhanced ship motion simulations that also include crash-ahead, crash-back, and astern motions, and to explore for which surge motions these quick calculations are reliable. The scope is limited to surge motion only, and therefore, the vessel only has one degree-of-freedom. The submarine is constrained in the other directions (no sway or yaw during the motion). Possibly, during the investigated maneuvers, the ship may be exposed to additional lateral forces generated by the propeller, rudder, and asymmetries in the flow around the ship advancing in the reverse direction. However, numerically modelling of each motion separately may introduce potential errors, and the simulation results for a ship performing combined motions would contain numerous sources of error. For this reason, to examine the effectiveness of the proposed method in the simplest form of the ship's surge maneuvers, the solutions are limited to surge motion only. The enhanced ship motion code, developed for this study, is expected to cover all the possibilities of the ship's surge motion. The represented methodology utilized into the code requires four-quadrant propeller hydrodynamics and uses this information to simulate crash-ahead, crash-back, and astern movements of the vessel. After the introductory information given in this section, Section 2 is devoted to the computational methodology of the CFD approach. These include ship resistance tests, open-water propeller tests, and free-running ship simulations. CFD simulations are used as a means to validate the practical methodology utilized into the code developed in this study, and the details of the approach are given in Section 3. Results are presented in Section 4, starting with the demonstration of ship resistance and four-quadrant ship propeller tests. The same section includes four distinct cases to present results obtained for all four-quadrant ship propeller hydrodynamics. The study is finalized with conclusions presented in Section 5.

2. Computational Methodology

The section describes the details of the numerical approach that was used in the computational fluid dynamics (CFD) part of the study.

2.1 Definition of the Problem

The paper covers the numerical modelling of the surge course of a free-running submarine during four different motion scenarios (straight-ahead, crash-ahead, crash-back, and astern). In order to predict these motions, two different numerical approaches were utilized: the in-house code based on the four-quadrant propeller performance, and the direct CFD. The former partially makes use of CFD results, as is extensively explained in the next section. The propeller performance diagram is utilized into the code by curve-fitting the obtained results. The latter models the flow around the hull with the aid of computational fluid dynamics by integrating the hydrodynamic performance of the propeller. All CFD calculations were conducted using the commercial software, Simcenter StarCCM+. In this study, there are three different CFD simulation approaches:

- Ship (submarine) resistance simulations
- Open-water propeller simulations
- Self-propulsion simulation considering the four different scenarios

The first one is for calculating the total ship resistance in order to validate the numerical towing tank model. The second approach is related to the open water tests of the propeller. Along with the validation purposes, these tests are also required to obtain the four-quadrant propeller performance characteristics. The third approach is for carrying out the free-running simulations of the submarine under aforementioned conditions (with virtual disk method representing the propeller). The details of the computational methodology are presented below with this order.

2.2 Ship Resistance Simulations

The benchmark submarine model generated by the Defense Advanced Research Projects Agency (DARPA) was used in the virtual towing tank tests. The geometry and the main perpendiculars of the DARPA form is presented in Figure 2 (left) and Table 1, respectively.

Table 1 Main dimensions of the DARPA AFF-8 submarine form

Parameter	**Dimension**
Length overall, L_{OA} (m)	4.356
Length between perpendiculars, L_{BP} (m)	4.261
Maximum diameter, D_{max} (m)	0.508
Wetted surface area, S (m^2)	6.348
Displacement volume, ∇ (m^3)	0.706

The computations were carried out in a Cartesian coordinate system with the origin in the model's aft peak. The negative x-axis is the incoming flow direction and the positive z-axis pointing upwards. The submarine is advancing with a constant forward speed in the positive x direction. The hull is fixed in other axes.

A rectangular shaped solution domain was created to solve the flow around DARPA hull. The submarine model was placed at the 4 L_{BP} and 6 L_{BP} away from the inlet and outlet boundaries, respectively. Sidewalls of the solution domain were extended to the length of 2 L_{BP} for spanwise direction and 2 L_{BP} for upward and downward direction from the center of the hull. The solution domain was established to be large enough to capture all of the changes in the flow field while complying with the ITTC recommendations [22]. The details of the solution domain can be seen in Figure 2 (right).

A uniform velocity profile which coincides with the hull velocity was imposed on the inflow boundary of the solution domain. At the outlet boundary, pressure outlet boundary condition was used. The body surface and the rest of the boundaries were treated with no-slip boundary condition. Second order scheme was applied for spatial discretization. The steady-state RANS simulations with well-known realizable κ-ε turbulence model [23] were performed to predict the resistance results. The previous research revealed that the submarine resistance results for steady translation can be obtained with high accuracy using steady analyses [17], [19], [24]. Thus, a steady RANS approach was adopted for resistance tests.

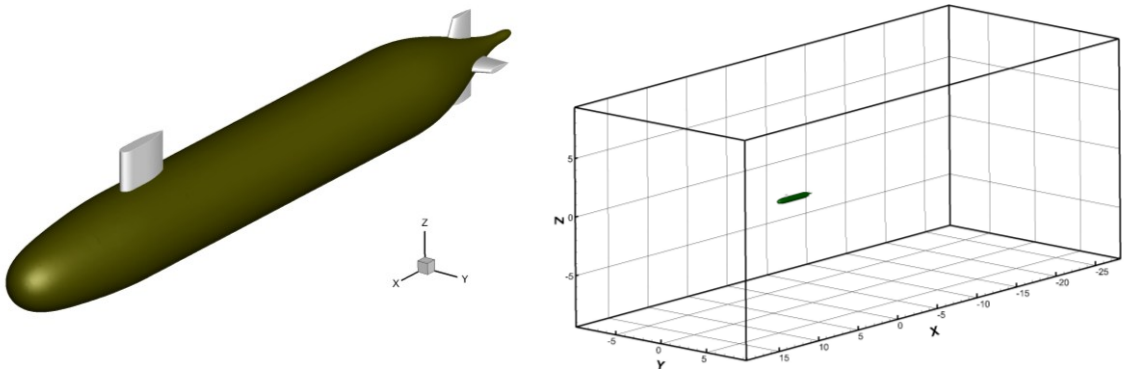

Fig. 2 The geometry of AFF-8 (fully appended) DARPA Suboff model (left). The details of the solution domain (right)

The solution domain was constructed using unstructured hexahedral elements. The general view of the grid topology is shown in Figure 3. The computational mesh was refined around the body with the aid of volumetric controls. Furthermore, additional refinement regions were created around the sail and the fins appended on the submarine stern. Also, grid structure was refined at the bow and wake regions to accurately capture the high velocity gradients and possible flow separations. While creating the surface grid, prismatic grid elements were positioned on the boundary layer along the submarine hull. To satisfy the requirement of wall function approach, the non-dimensional wall distance values were kept in the range of $30 < y^+ = \frac{u_t y}{v} < 300$ where u_t is the friction velocity, y is the height of the first cell on the wall and ν is the kinematic viscosity of the fluid. Total number of the mesh count was 0.98 M for resistance simulations.

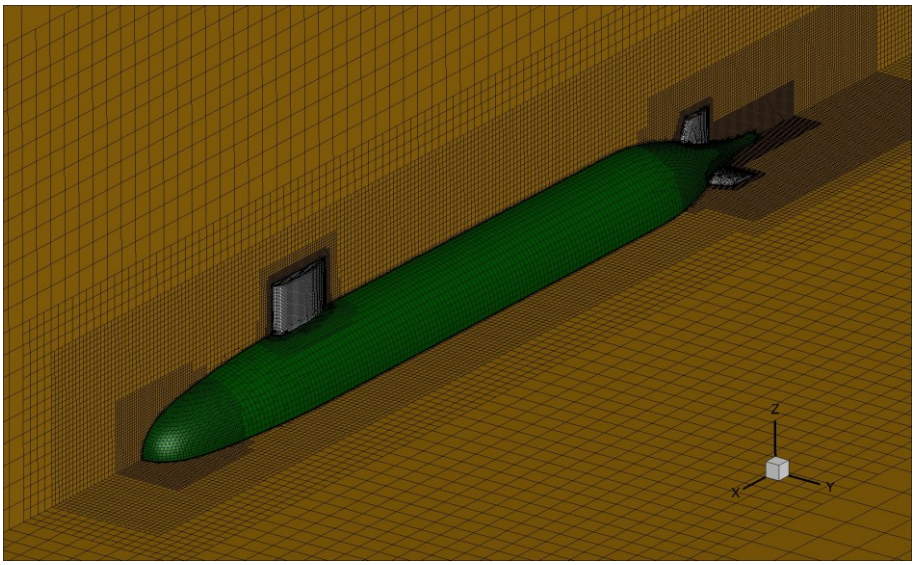

Fig. 3 The grid structure around the submarine hull

2.3 Open-water Propeller Test Simulations

A series of open-water propeller simulations were conducted to obtain the performance curves of the propeller. Along with validation purposes, the predicted propeller results serve as input data for the propulsion predictions with our in-house code. E1619 propeller geometry introduced by INSEAN was considered in the computations [1]. The geometry of the propeller and the main particulars are shown in Figure 4 and Table 2, respectively.

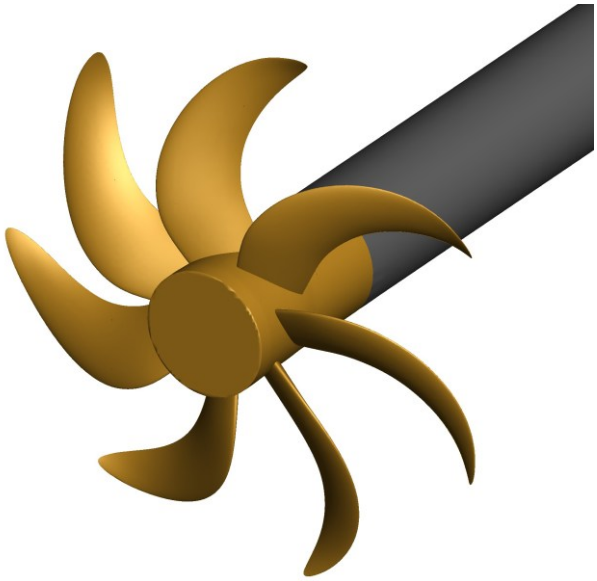

Fig. 4 The geometry of the INSEAN E1619 propeller

Table 2 Main dimensions of the INSEAN E1619 propeller

Parameter	**Dimension**
Diameter, D (m)	0.485
Number of blades, Z	7
Hub diameter ratio, D_H / D	0.226
Pitch at $r = 0.7R$	1.15
Chord at $0.75R$ (m)	0.0068
Rotation	Right Hand

A similar numerical towing tank procedure used in resistance tests was adopted in open-water propeller simulations. A cylindrical-shaped solution domain was created around the body. The inflow boundary and sidewalls were placed at 5D, and the outlet boundary was placed at 10D distance away from the propeller. The sliding mesh (or Rigid Body Motion) technique was used to simulate the propeller rotation. While this method is regarded as quite precise for simulating propeller rotation, it is highly time-consuming in terms of computational resources [21]. To utilize the sliding mesh technique, the open water analyses were conducted in an unsteady manner. The time-step size in these cases corresponds to the 3 degrees of rotation of the propeller. In order to achieve different advance ratios (J) within the same numerical configuration, the propeller's rotational speed was fixed, and the incoming flow velocity was adjusted accordingly. The grid structure, shown in Figure 5, was precisely constructed for the accurate prediction of the swirly flow around the propeller. The grid structure was refined in the vicinity of the propeller. The refinement region was extended through the propeller slipstream, to capture the high velocity gradients in the propeller wake. A smooth mesh transition was provided along both sides of the sliding mesh interface, in order to minimize possible numerical errors. The surface mesh was structured fine enough for the successful representation of

the high curvatures in the propeller geometry. The wall $y+$ values along the propeller surface was changing according to the advance ratio, however, the mean value stays in the range of 60 to 100.

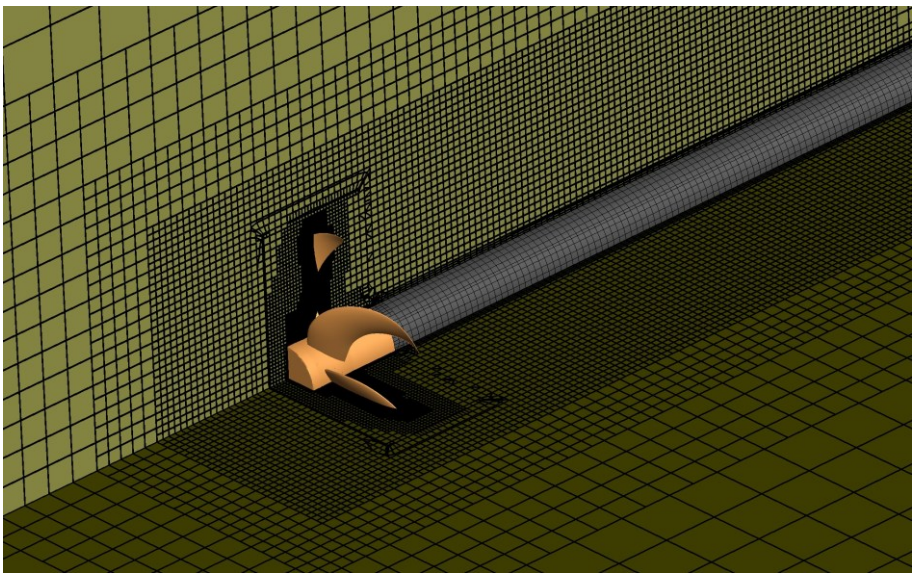

Fig. 5 Mesh structure around the propeller in open-water conditions

2.4 Free-running Simulations

Free-running test simulations of the submarine model was conducted to assess the performance of the vessel under aforementioned conditions. Free-running simulations enable the ship to navigate freely, under the effect of propulsion forces and the surrounding environment. Unlike the traditional surge-fixed numerical set-ups, free-running models are capable of simulating real-time ship course without any limitations by releasing the ship's surge freedom [25]. In this study, the course of the submarine was modelled using overset grid technique. For this purpose, the numerical towing tank model in resistance tests was modified to adopt the overset grid. First, the solution domain was split into two regions: the static background region and the overset region that travels together with the body. The configuration is shown in Figure 6. With this, the overset grid enables the real physical translation of the body. It should be noted that, due to the physical movement of the vessel, it became necessary to expand the solution domain along the projected travel path, ensuring it adequately covered the distance of the submarine's motion. Consequently, during free-running simulations, the inflow boundary of the domain, as employed in resistance tests, was strategically repositioned further downstream, depending on the submarine's velocity.

In free-running simulations, the propulsive force accelerates the ship forward, while the overall hydrodynamic resistance acts to decelerate the ship. In this study, the interaction between the flow and the moving body was simulated by integrating the Dynamic Fluid Body Interaction (DFBI) model. The model computes the net forces acting on the body at certain intervals. By incorporating these values into the equations of motion, the model determines the ship's new position until the body reaches an equilibrium. In this study, no velocity input is defined for the boundaries of the solution domain. The initial velocity (zero or a constant value) is prescribed for the body itself using the DFBI module. Subsequently, the submarine continues its motion solely by its own dynamics.

In this study, the submarine model was set free to move in surge direction (+/- x translation) and kept fixed for other motions. The unsteady simulations were performed to model the translation of the submarine in free-running tests. The time step value Δt is determined as $1x10^{-2}$. This value also complies with the recommendations of ITTC guideline [26] for the maximum speed achieved in each scenario.

The propulsive force of the propeller was included in the calculations using body force (virtual disk) method. The body force method simplifies the hull-propeller combination model by representing the features of the propeller as a body force [27]. To do this, the method applies the propeller performance curves to a virtual thin cylindrical disc located at the propeller's position. In the cases where detailed propeller flow is

not essential (excluding cases like the interaction between propeller-hull-rudder system), the body-force method aids in reducing the numerical complexity and the computational cost of the self-propulsion calculations [28]. Besides, in cases where lateral force and motions are not dominant (like surge velocity), the model provides quite good results and enables relatively rapid computation [29]–[31]. The thrust and torque coefficient curves calculated in open-water propeller simulations were used in body force calculations. Note that the body force model was used in combination with the DFBI module to simulate the impact of the propeller.

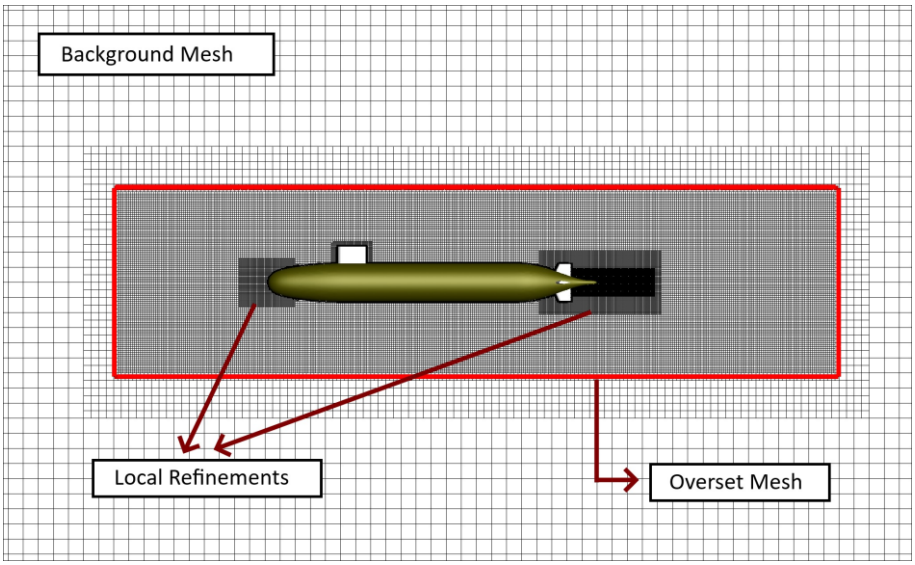

Fig. 6 The overset grid configuration in free-running simulations

The grid topology in the free-running simulations were similar to the bare hull resistance computations. A uniform distribution of refined grids was applied through the whole overset region. The grid size in the overset region was 1/4 of those in the background region. Additional refinements were applied to the critical regions such as the wake, the bow and the appendages. The grid structure of the overset free-running simulations can be seen in Figure 6.

3. The Mathematical Background of the Code

The surge motion of the ship is predicted using the propeller hydrodynamic performance diagram by our in-house code, ship motions with four-quadrant propeller, shortly named as SMot4QP. The code also makes use of the ship resistance test results and is an enhanced version of the code based on self-propulsion estimation (SPE) method, published previously in various studies such as [19], [20], [32]. Other than the conventional self-propulsion case (the straight-ahead case), the code is able to simulate crash-ahead, crash-back, and astern motions. Ship resistance and open-water propeller tests are simulated via CFD and the results are given as input to SMot4QP. The adopted procedure is shown in Figure 7.

This section explains the theoretical background of SMot4QP in-house code. For a body in motion with a total mass m_T and a forward speed V, Newton's second law of motion is given by:

$$F = \frac{d(m_T V)}{dt} \tag{1}$$

We assume that the total mass is not changing during motion. In the case of a ship moving in water, the total mass can be expressed by summing up its displacement tonnage m and the added mass m_x. In this case, equation (1) becomes:

$$F = (m + m_x) \cdot \frac{dV}{dt} \tag{2}$$

Numerical form of this equation can be written by:

$$F \cdot \Delta t = (m + m_x) \cdot \Delta V \tag{3}$$

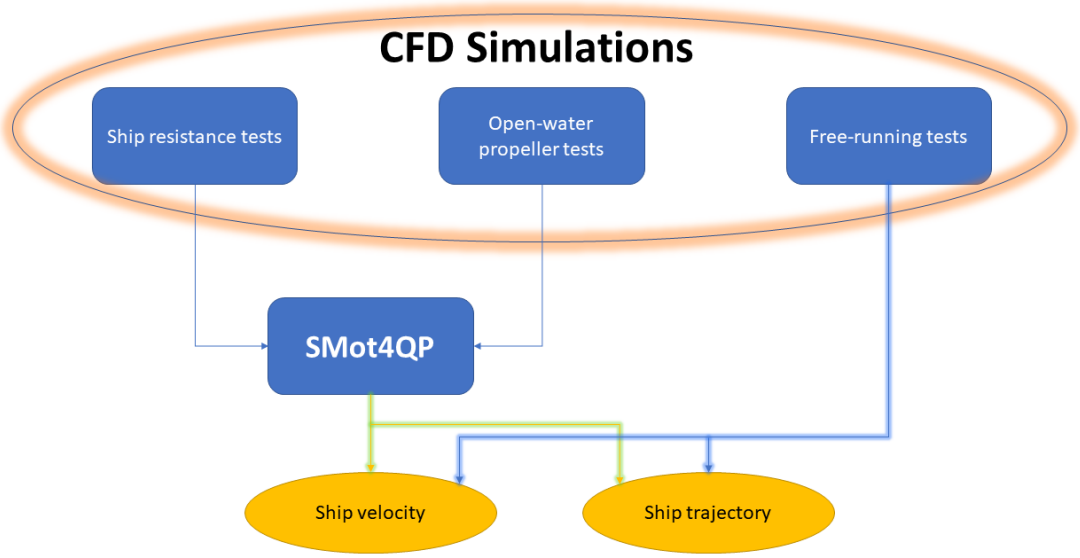

Fig. 7 Procedure used in this study. The in-house code uses CFD simulation results as input to generate the ship's velocity and trajectory.

A code is developed that uses equation (3) to calculate the ship's surge velocity during its straight-ahead course. The purpose of this code is to compute the surge speed and position for ships that exhibit a single degree-of-freedom (1DOF). Comprising a primary segment and two supplementary functions, the code requires input of the hydrostatic and geometric features of the ship, its resistance curve, and four-quadrant propeller performance. The simulation initiates from the user-provided initial speed and position.

Upon inputting the necessary data, the primary segment first determines the added mass through the utilization of Clarke's empirical relation (1983). Thereafter, the simulation loop commences, and the subsequent computations are performed in the designated order:

- Time
- Velocity received by the propeller
- Advance ratio
- Coefficients of propeller thrust and ship resistance (function 1)
- Thrust coefficient
- Thrust
- Ship Resistance
- Skin friction correction (function 2)
- Ship velocity
- Ship's position

The time is calculated at each iteration using the time step size Δt, which is given as an input. The equation used to determine the velocity received by the propeller V_A is:

$$V_A = V \cdot (1 - w) \tag{4}$$

where V denotes the ship's speed and w is the wake fraction. The wake fraction (w) is a dimensionless parameter that quantifies the effect of the ship's hull on the flow of water entering the propeller and can be calculated using resistance analyses. The advance coefficient is calculated by

$$J = \frac{V_A}{nD} \tag{5}$$

In this equation, n is the propeller rotation rate and D is the propeller diameter. Following this step, the primary segment proceeds to call function 1, which encompasses the ship resistance and propeller performance characteristics. The function works in four quadrants.

- The 1st quadrant is the ahead condition where the ship speed and propeller rotation rate are positive (the ship moves forward with designated propeller rotation).
- The 2nd quadrant is the crash-ahead condition in which the propeller rotation rate is positive but the ship speed is negative (the ship moves backwards with designated propeller rotation
- The 3rd quadrant is the crash-back condition where the ship speed is positive but the propeller rotation rate is negative (the ship moves forward but the propeller is working reversed).
- The 4th quadrant is the astern condition in which the ship speed and the propeller rotation rate are both negative (the ship is moving backwards with reversed propeller rotation).

After necessary parameters are extracted from function 1, the primary segment calculates the thrust coefficient utilizing the equation:

$$K_T = k_0 + k_1 \cdot J + k_2 \cdot J^2 \tag{6}$$

and the thrust by:

$$T = K_T \rho n^2 D^4 \tag{7}$$

The coefficients of ship resistance, extracted from function 1, is used to calculate the total resistance by the following equation:

$$R_T = r_1 \cdot V + r_2 \cdot V^2 \tag{8}$$

The ship moves forward at a certain speed where the propeller thrust, and the ship resistance achieve a state of equilibrium. However, this equilibrium state differs in scaled ships due to variations in skin friction resulting from significant differences in Reynolds numbers [33]. Skin friction correction arises from differences in Reynolds numbers between model and full-scale ships. The ITTC addresses this extrapolation using the ITTC 57 Model-Ship Correlation Line (which is originated from the ATTC line $0.242/\sqrt{C_F} = \log_{10}(Re \cdot C_F)$) . For further details, please refer to page 4 of ITTC 7.5-02-02-03 [34]. To account for this, the primary segment calls function 2. This function calculates the skin friction correction which may or may not be necessary depending on the scale of the ship. If the user works with a full-scale ship, then this function is omitted. If the user prefers to work with a mode-scale ship, then this function:

- first computes the Reynolds numbers Re of both the model and the full-scale ship,
- then calculates the frictional resistance coefficient C_F of both the model and the full-scale ship using ITTC 1957 correlation line formula,
- and finally calculates the skin friction correction F_D.

To accomplish these steps, function 2 uses the following formula:

$$Re = \frac{\rho V L}{\mu} \tag{9}$$

$$C_F = \frac{0.075}{(\log Re - 2)^2} \tag{10}$$

$$F_D = \frac{1}{2} \rho S V^2 (C_{Fm} - C_{Fs}) \tag{11}$$

In these equations L is the ship length, S is the wetted surface area, and C_{Fm} and C_{Fs} denote the frictional resistance coefficients of model and full-scale ships, respectively. ρ is the water density and μ is the dynamic viscosity.

Furthermore, although SMot4QP has the capability to include skin friction correction via function 2, it was not necessary for our simulation case. This is because we calculated the model's self-propulsion rather than the full-scale ship's self-propulsion.

After all above is completed, the ship velocity can be defined by rearranging equation (3) and stating it in the form:

$$V_i = V_{i-1} + \frac{\Delta t}{m+m_x} \cdot \left(T + F_D + \frac{R_T}{1-t}\right) \tag{12}$$

Here, t is the thrust deduction factor. The thrust deduction factor (t) is a dimensionless parameter that quantifies the reduction in the effective thrust produced by the propeller due to the interaction between the propeller and the hull. In the present study, the propeller-hull interaction parameters, wake fraction (w) and thrust deduction factor (t), were assumed to be constant in all calculations.

Finally, the position of the ship x is calculated by:

$$x_i = x_{i-1} + V_i \cdot \Delta t \tag{13}$$

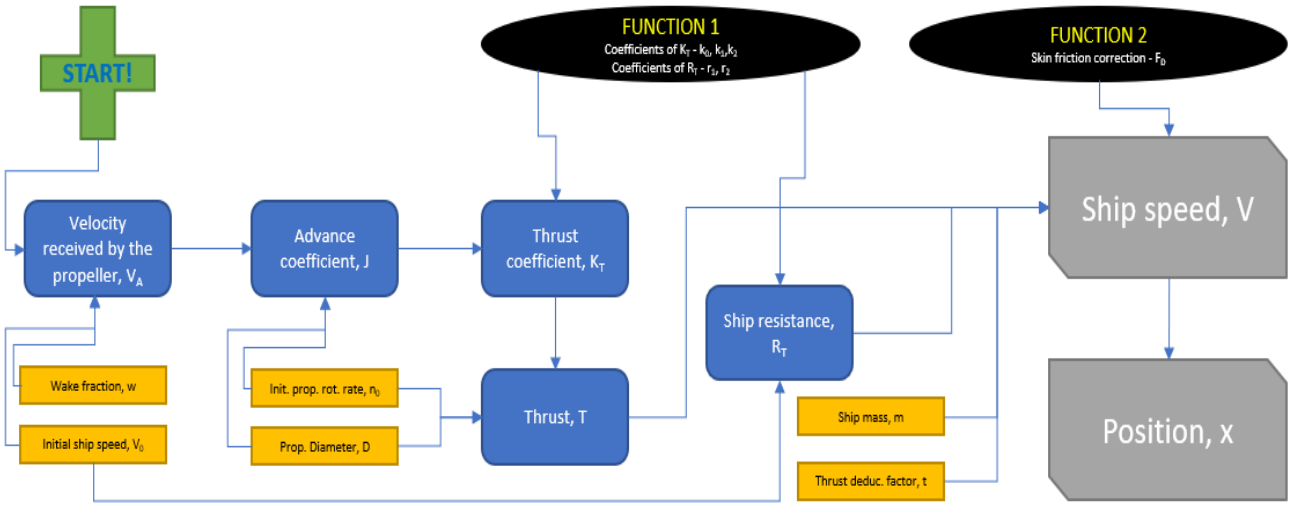

Fig. 8 The flow diagram of the SMot4QP code

Figure 8 displays the flow diagram of the code. The inputs are represented by rectangles with an orange background, while the outputs, which include the speed and location of the ship, are denoted by rectangles with a grey background. The primary segment of the code, which is responsible for calculating the blocks, is distinguished by a blue background. The two functions called by the primary segment are shown by ellipses with black background.

4. Results

This section presents the results obtained from the CFD computations, along with the predictions made using our in-house code, SMot4QP. The section begins by presenting the simulation results of ship resistance and open-water propeller tests. Subsequently, the four-quadrant propeller results are showcased, which serve as the foundation for the SMot4QP predictions across four distinct cases encompassing straight-ahead, crash-ahead, crash-back, and astern ship motions.

4.1 Ship Resistance Tests

A series of ship resistance tests were conducted on the DARPA AFF-8 submarine form in order to evaluate the accuracy of the numerical approach used in computational fluid dynamics (CFD) calculations. The results of these simulations are depicted in Figure 9 (left), illustrating the predicted resistance components. To validate the numerical approach, the total resistance values were compared with the towing tank measurements conducted by Liu and Huang [35]. It was found that the numerical results closely matched the experimental ones for all forward velocities, indicating excellent agreement.

We also examined the resistance components to further validate the numerical approach. The figure reveals that the calculated frictional resistance values closely align with the data obtained using the ITTC-

1957 frictional correlation line [36]. Expectedly, frictional resistance constitutes the primary component of hull resistance. Viscous pressure resistance results were compared with those presented in the study conducted by Kinaci et al.[19]. The results indicate very good agreement between the predicted RVP of the submarine model and the findings of the aforementioned study.

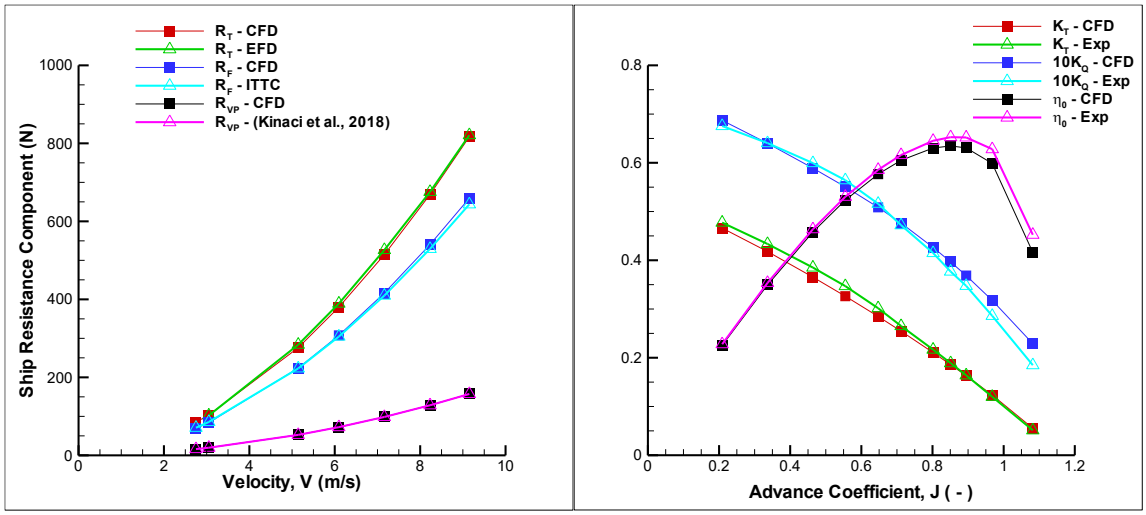

Fig. 9 Validation of CFD results for ship resistance (left) and open-water propeller tests (right)

Along with the validation of the present predictions with experimental data, a verification study was performed to evaluate the uncertainty of the numerical results of resistance test using the Grid Convergence Index (GCI) technique based on the Richardson extrapolation method. This method was first suggested by [37] and has been widely employed in the ship hydrodynamics literature using the procedure provided by Celik et al. [38].

N_1, N_2 and N_3 are the total number of grids applied for the numerical computations and h_1, h_2 and h_3 are the grid sizes. ΔV_i represents volume of the ith and the refinement ratios r_{21} and r_{32} are defined by the following expressions:

$$r_{21} = \frac{h_2}{h_1} \tag{14}$$

$$r_{32} = \frac{h_3}{h_2} \tag{15}$$

$$h_j = \left[\frac{1}{N_j}\sum_{i=1}^{N_j}(\Delta V_i)\right]^{1/3}, j = 1,2,3 \tag{16}$$

It should be considered that according to the Celik et al. [38] , the refinement ratio is recommended to be greater than 1.3. In this study, a refinement ratio of $\sqrt{2}$ was chosen, which is usually applied in CFD applications. The difference between the solution scalars (ε) can be calculated according to the following equation:

$$\varepsilon_{21} = \varphi_2 - \varphi_1, \quad \varepsilon_{32} = \varphi_2 - \varphi_1 \tag{17}$$

where $\varphi_1, \varphi_2, \varphi_3$ denote the numerical results for coarse, medium, and fine grid, respectively. The solution scalar was set as the dimensionless total resistance coefficient of the submarine model at service speed $V = 3.051$ m/s.

The following equation can be used to determine the extrapolated value:

$$\varphi_{ext}^{21} = \frac{(r^p\varphi_1 - \varphi_2)}{(r^p - 1)} \tag{18}$$

Here p is the apparent order of the method and calculated using the following equation:

$$p = \frac{1}{\ln(r_{21})}\left|ln|\varepsilon_{32}/\varepsilon_{21}| + q(p)\right| \tag{19}$$

$$q(p) = ln\left(\frac{r_{21}^p - s}{r_{32}^p - s}\right) \tag{20}$$

$$s = sgn(\varepsilon_{32}/\varepsilon_{21}) \tag{21}$$

The approximate relative error (e_a^{21}) and extrapolated relative error , (e_{ext}^{21}) can be defined as follows:

$$e_a^{21} = \left|\frac{\varphi_1-\varphi_2}{\varphi_1}\right|, \quad e_{ext}^{21} = \frac{|\varphi_{ext}^{21}-\varphi_1|}{\varphi_{ext}^{21}} \tag{22}$$

Eventually, grid convergence index can be obtained as follows:

$$GCI_{fine}^{21} = \frac{1.25e_a^{21}}{r_{21}^p-1} \tag{23}$$

Table 3 presents the uncertainty level computed for the DARPA Sub-off submarine model utilized in the numerical simulations. According to the uncertainty analyses results, the uncertainty is calculated to be approximately 0.6%.

Table 3 Grid convergence for total resistance coefficient.

Parameter	Value
N_1, N_2, N_3	2248701, 979909, 451840
r_{21}, r_{32}	1.319, 1.294
φ_1, φ_2, φ_3	0.00347, 0.00351, 0.00364
ε_{21}, ε_{32}	0.000038, 0.000128
R	0.298
q	0.091
p	4.468
$\varphi_{ext}^{21}, \varphi_{ext}^{32}$	0.003458, 0.003459
e_a^{21}, e_a^{32}	0.0110, 0.03658
$e_{ext}^{21}, e_{ext}^{32}$	0.004527, 0.015180
GCI_{MEDIUM}^{32}	0.018690
GCI_{FINE}^{21}	0.005634
GCI_{MEDIUM}^{32} (%)	1.86
GCI_{FINE}^{21} (%)	0.56

In addition to the uncertainty analysis, a mesh dependency study was also performed. The results are shown in Table 4. considering both accuracy and computational cost of the solutions, medium mesh was selected for the rest of the calculations

Table 4 The summary of the mesh dependency study

	EFD	Coarse	Medium	Fine
Grid number	-	451840	979909	2248701
C_T (x10^{-3})	3.467	3.640	3.505	3.473
Relative error	-	%4.98	%1.09	%0.17

4.2 Open-water Propeller Tests

We have conducted open-water propeller tests to compare our numerical results with experiments. Conventional open-water tests operate in the 1st quadrant of the propeller, in which the submarine is moving forward and the propeller is rotating regularly. Numerical results in comparison with the experiments of [1] are given in Figure 9 (right). Thrust coefficients are in excellent accordance with the experiments at high

advance ratios, although there are slight differences at lower advance ratios. The torque coefficient demonstrates a very good agreement in low advance ratios and slightly overpredicts in high J. As for the open-water propeller efficiency, the level of agreement achieved is deemed satisfactory. In general, CFD calculations produce very acceptable performance coefficients for the propeller, with slight differences in low loads (high J). As pointed out by Chase and Carrica [1] the discrepancies between the CFD and EFD results could stem from various factors, including errors due to differences in geometry or the presence of the driving mechanism for the shaft or walls in the towing tank, which were not accounted for in the CFD computations.

4.3 Conventional Self-Propulsion Analyses

To expand the validation studies of the numerical setup established to determine the performance of the submarine in surge motion scenarios, a conventional self-propulsion analysis was performed. The self-propulsion analysis is conducted to determine the propulsive force and propulsion characteristics of the submarine moving at a prescribed advance speed. The method used in the self-propulsion analyses is detailed by Kinaci et al. [19] and Cosgun [3]. The analysis conducted at a submarine advance speed of V=2.75 m/s for validation purposes and the results are presented in Table 5 in comparison with Chase [39]. The results show high agreement with each other in terms of both propulsion characteristics and the advance ratio in the self-propulsion condition.

Table 5. Self-propulsion characteristics of DARPA at V=2.75 m/s

		K_T	$10K_Q$	η_0	J
Chase [39]	Self propelled	0.2342	0.4714	-	-
	Using CFD OWC	0.2342	0.4577	0.6115	0.7498
	Using Experimental OWC	0.2342	0.4353	0.6602	0.7659
Present study	Self propelled	0.2389	0.4646	-	-
	Using CFD OWC	0.2389	0.4586	0.6141	0.7435
	Using Experimental OWC	0.2389	0.4411	0.6318	0.7604

4.4 Four-quadrant Ship Propeller Performance

As mentioned in the previous section, the four-quadrant ship propeller performance is required in the code to calculate the ship surge velocity. In this section; we outline the possible surge motions of the ship, the direction of rotation of the propeller, and present the hydrodynamic performance of the fitted propeller to DARPA Suboff in four quadrants.

Table 6 Curve fitted equations of the thrust coefficients for four-quadrant propeller performance

1st quadrant	Ahead	$V_A > 0$	$n > 0$	$K_{T_1} = -0.1833J^2 - 0.2235J + 0.5095$
2nd quadrant	Crash-ahead	$V_A < 0$	$n > 0$	$K_{T_2} = 0.4109J^2 + 0.4706J + 0.5140$
3rd quadrant	Crash-back	$V_A > 0$	$n < 0$	$K_{T_3} = -0.4207J^2 - 0.1765J - 0.1758$
4th quadrant	Astern	$V_A < 0$	$n < 0$	$K_{T_4} = 0.2722J^2 - 0.0041J - 0.1640$

A forward-going ship is working in the 1st quadrant. In this case, the propeller is working conventionally, n>0, and the ship is moving ahead, V_A>0. If this ship is to decrease her speed, then the propeller starts working reversed. This is the crash-back condition where the ship is still moving forward but with a decreased speed, V_A>0, and the propeller rotation is reversed, n<0. This corresponds to the 3rd quadrant of propeller performance. As the propeller works reversed, the ship will reach zero speed and at some point, she

will eventually start moving astern. In this case, the propeller rotation direction is still negative, $n<0$, and the ship is moving backwards, $V_A<0$. This is the 4th quadrant. The propeller works in the 2nd quadrant once she needs to move forward once again. This time, the ship is still moving backwards, $V_A<0$, but the propeller is rotating in positive direction, $n>0$. All this information is summarized in Table 6 for INSEAN E1619 propeller.

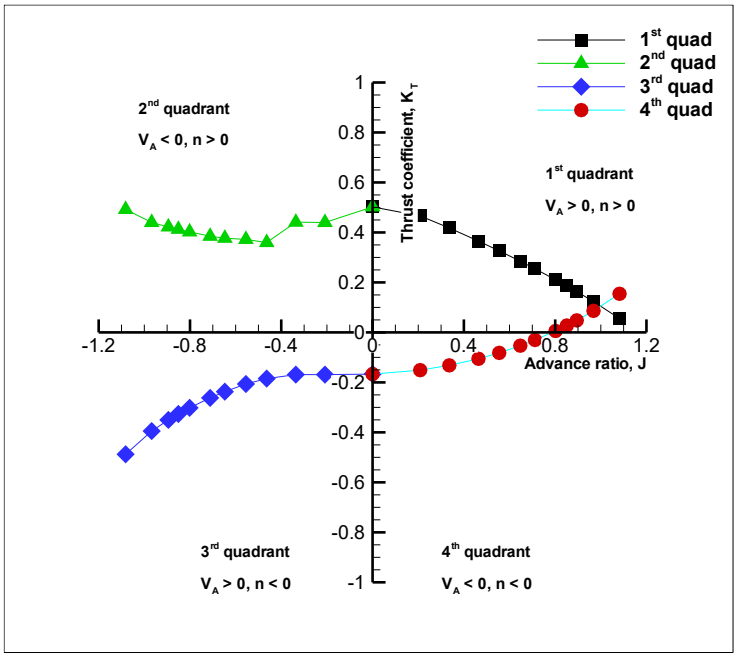

Fig. 10 Four-quadrant propeller thrust coefficient

Curve fitted equations for the thrust coefficient K_T for four-quadrant propeller performance are given in Table 6. The graphed version of these equations is given in Figure 10.

We have identified four different cases for each ship motion type (straight-ahead, crash-ahead, crash-back, and astern). For each of these cases we have simulated the submarine velocity and position in the time domain using our ship motion code with four-quadrant propeller performance and utilizing direct CFD simulations. The simulation scenarios with initial velocity and propeller rotation rate are listed in Table 7.

Table 7 Simulation scenarios and associated ship motion type

	Unit	*Case #1*	*Case #2*	*Case #3*	*Case #4*
Initial Velocity	m/s	0	-3	5	0
Propeller Rotation Rate	rps	20	20	-5	-3
Associated Propeller Quadrant		1	2	3	4
Ship Motion Type		Straight-ahead	Crash-ahead	Crash-back	Astern

4.5 Case#1 – Straight-ahead Motion

The first case involves the self-propulsion case of DARPA Suboff. Here, the submarine is initially at rest, and the propeller rotates at a rate of 20 revolutions per second. As a result, the submarine accelerates and attains a positive steady vessel speed. The propeller operates in the first quadrant in this case. Figure 11 illustrates the simulation results in the time domain.

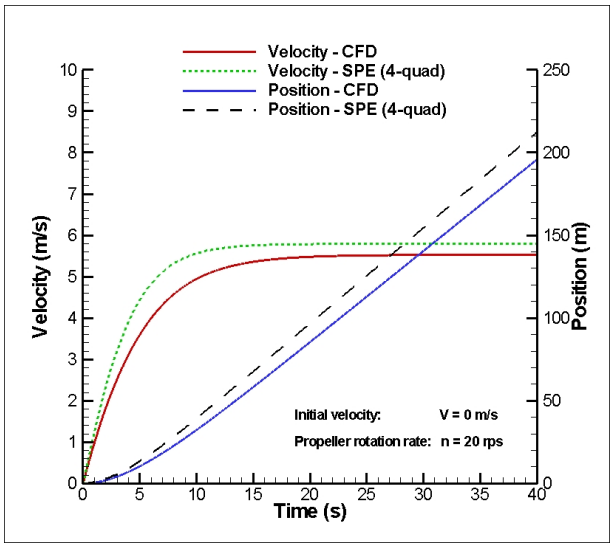

Fig. 11 Simulation results for Case#1 – Straight-ahead

The final speeds reached in both calculations are quite close. The SMot4QP simulation predicts a steady submarine velocity of 5.79 meters per second over a 40-second period, whereas direct CFD predicts a velocity of 5.53 meters per second. The difference in results is around 4%. Since the velocity is higher in SMot4QP, the submarine covers 17 meters more distance than predicted by CFD. The difference between final position reached in both simulations are less than 10%.

4.6 Case#2 – Crash-ahead Motion

In the second case, the submarine is initially moving in the backwards direction with a velocity of -3 meters per second, and the propeller again rotates at 20 revolutions per second. We expect the submarine to move astern initially due to the negative ship speed, but as the speed increases, the ship reaches zero velocity and then accelerates to a positive speed. This case is similar to the first case, but with a different initial speed.

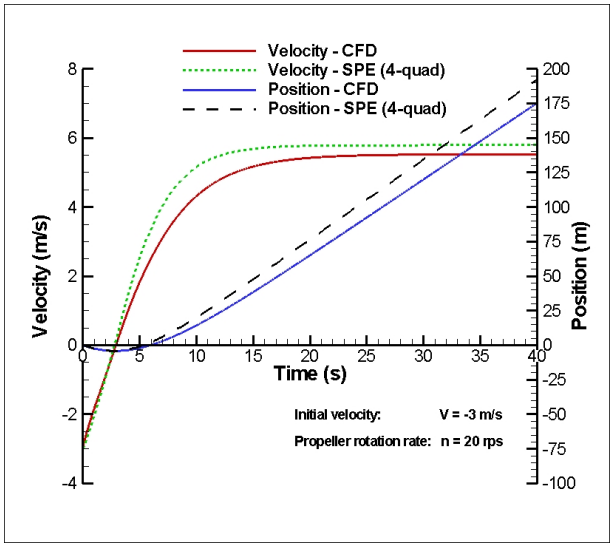

Fig. 12 Simulation results for Case#2 – Crash-ahead

Similar to the previous case, the simulation ends after 40 seconds, and the results are comparable to those of the first case. Time-based simulation results are given in Figure 12. Both calculation methods produce very close predictions in term of final speed achieved. The steady state speeds predicted by SMot4QP and CFD are 5.79 and 5.53 meters per second, respectively, with a difference of 17 meters between the two simulations. The only difference between the two cases is that the submarine moves backward for the first

5 seconds in the crash-ahead motion case, covering a distance of 4 meters in that time frame. The submarine takes about 2.5 to 3 seconds to reach zero velocity in both simulations before accelerating to a positive speed.

4.7 Case#3 – Crash-back Motion

In the third case, the submarine is initially moving forwards with a velocity of 5 meters per second but the propeller is rotating reversed at a rate of 5 revolutions per second. The submarine moves forward due to its initial speed; however, it loses its velocity due to the reversed propeller rotation and starts going backwards after some time. Results are depicted in Figure 13.

In this scenario, the propeller is not only operational within the third quadrant but is also undergoing a transition from the third quadrant to the fourth quadrant. The submarine's velocity turns negative using both methods, and this is when we contemplate the occurrence of this transition. The simulation lasts after 150 seconds and our in-house code generates a velocity of -1.87 meters per second while CFD prediction is -1.74 meters per second. The difference is about 7%. The final speeds predicted by the two calculation methods are very close, on the other hand the differences in the acceleration processes lead to significant discrepancies in the position histories. In the crash-back case, the submarine transitions between positive and negative speeds, exposing it to variable wake effects. In the present study, the propeller-hull interaction parameters, wake fraction (w) and thrust deduction factor (t), were assumed to be constant throughout the calculations performed with SMot4QP. Thus, the SMot4QP code does not account for variable wake effects, which probably the reason for the discrepancies between the acceleration process of the calculation methodologies.

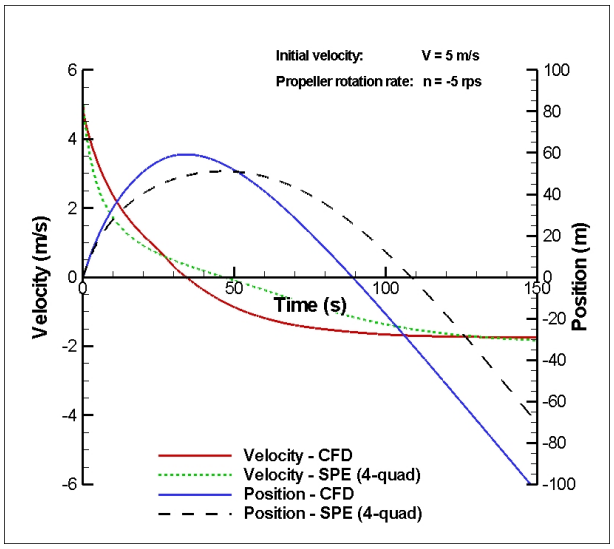

Fig. 13 Simulation results for Case#3 – Crash-back

4.8 Case#4 – Astern Motion

The fourth case is the astern motion of the submarine, in which the motion starts with zero submarine speed initially and the propeller is working reversed at a rate of 3 revolutions per second. The initially stationary submarine starts moving backwards due to reversed propeller rotation. Results are shown in Figure 14.

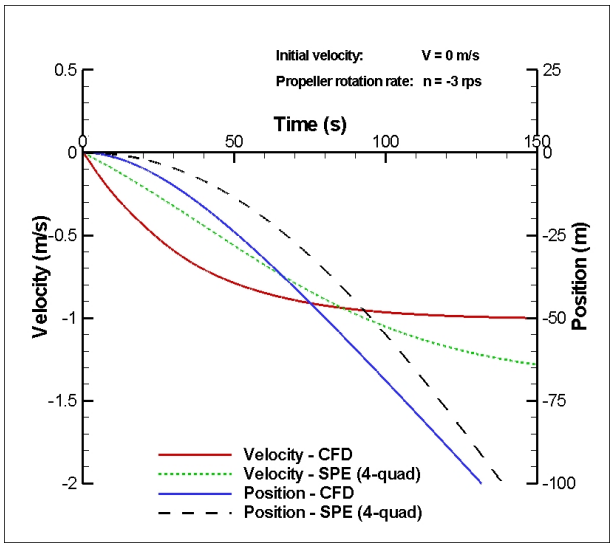

Fig. 14 Simulation results for Case#4 – Astern

The figure depicts 150 seconds of the simulation and SMot4QP still has not reached steady state velocity. On the other hand, CFD generates a steady state submarine speed of -1.01 meters per second. A remarkable disparity is observed between the obtained results, and this discrepancy is further manifested in the misprediction of the self-propulsion point during the astern motion. CFD finds the self-propulsion point as J_{CFD}=0.94, while the in-house code result is J_{CFD}=1.23. It should be noted here that the advance ratio for this specific case is very high. Upon observing the 4th quadrant results of the propeller performance given in Figure 10, it can be seen that despite working reversed, the propeller produces a positive thrust in this case.

The other point worth it to mention is the translation direction of the submarine. In the straight-ahead and crash-ahead maneuvers, where the submarine moves forward, the final speeds reached in both calculations are quite close. However, in the astern maneuver, where the submarine moves backward, this difference is significantly larger compared to the other cases. Similarly, in the crash-back case, where the submarine partially moves backward, even though the final speeds predicted by the two calculation methods are very close, there are notable discrepancies observed in the acceleration processes. It should be kept in mind that the SMot4QP uses resistance values obtained during the forward movement of the submarine. The resistance characteristics of the submarine are expected to differ when moving in reverse compared to forward motion. This difference contributes to the error rate observed during the submarine's reverse maneuvers.

5. Conclusion

A ship's hydrodynamic performance can predicted by computationally expensive direct CFD simulations or by costly free-running model tests. Nevertheless, the industry needs quick assessment methods, especially in the preliminary design stage, to facilitate more efficient propulsion system designs or to integrate the ship into modern applications such as autonomous operation or dynamic positioning. Various methods exist to expedite computations; however, traditional ship propulsion assessments have solely focused on steady forward motion with a regular direction of propeller rotation. This study aims to broaden the scope to include various surge motions such as crash-ahead, crash-back, and astern movements. To address this, we propose a practical approach by introducing an in-house developed simulation code that predicts ship hydrodynamic performance under different conditions by utilizing a four-quadrant propeller performance and ship resistance test results. While the study primarily focuses on submarines, the code's versatility makes it applicable to various types of vessels. Our calculations show improved accuracy for straight-ahead and crash-ahead motions. In these cases, the final speeds obtained from the current method closely resemble those obtained from direct CFD calculations. However, for the astern and crash-back cases, where the submarine fully or partially moves backward, the discrepancy between two methods becomes more pronounced compared to the other scenarios. This indicates a need for further improvement in modeling propeller-ship interaction and wake calculations in these specific maneuvers.

The method proposed in this paper is anticipated to play a pivotal role in improving the accuracy of ship motion predictions. Conventional maneuvering models are limited, as they only consider propeller thrust in the first quadrant. However, ship and propeller movement/rotation in adverse directions creates four distinct propulsion modes. Accurate prediction models for these unconventional ship motions require incorporating the forces acting on the ship and generated by the propeller due to all these propulsion modes. For this reason, mathematical models of dynamic positioning systems lack the necessary comprehensiveness for such simulations. For this reason, mathematical models of dynamic positioning systems fall short of comprehensive simulations. The code developed in this study can integrate with six degree of freedom ship motion codes and augment the precision of navigation and control of marine vehicles. We plan for our future studies to focus on in this particular direction, and conduct relevant experiments to further validate the model.

ACKNOWLEDGEMENTS

The third author was supported by Scientific Research Projects Department of Istanbul Technical University. Project Number: 44879.

REFERENCES

[1] Chase, N., Carrica, P.M., 2013. Submarine propeller computations and application to self-propulsion of DARPA Suboff. *Ocean Engineering*, 60, 68–80. https://doi.org/10.1016/j.oceaneng.2012.12.029

[2] Zhang, N., Zhang, S.L., 2014. Numerical simulation of hull/propeller interaction of submarine in submergence and near surface conditions . *Journal of Hydrodynamics*, 26(1), 50–56. https://doi.org/10.1016/S1001-6058(14)60006-8

[3] Cosgun, T., 2021. Numerical Self-Propulsion Assessment of a Generic Submarine Model at Various Forward Speeds. *Journal of ETA Maritime Science*, 9(3), 192–199. https://doi.org/10.4274/jems.2021.24654

[4] Doğrul, A., 2019. Hydrodynamic Investigation of a Submarine Moving Under Free Surface. *Journal of ETA Maritime Science*, 7(3), 212–227. https://doi.org/10.5505/jems.2019.42204

[5] Gaggero, S., Villa, D., Viviani, M., 2017. An extensive analysis of numerical ship self-propulsion prediction via a coupled BEM/RANS approach . *Applied Ocean Research*, 66, 55–78. https://doi.org/10.1016/j.apor.2017.05.005

[6] Jasak, H., Vukčević, V., Gatin, I., Lalović, I., 2019. CFD validation and grid sensitivity studies of full scale ship self propulsion. *International Journal of Naval Architecture and Ocean Engineering*, 11(1), 33–43. https://doi.org/10.1016/j.ijnaoe.2017.12.004

[7] Mikulec, M., Piehl, H., 2023. Verification and validation of CFD simulations with full-scale ship speed/power trial data. *Brodogradnja*, 74(1), 41–62. https://doi.org/10.21278/brod74103

[8] Saydam, A.Z., Küçüksu, G.N., İnsel, M., Gökçay, S., 2022. Uncertainty Quantification of Self-Propulsion Analyses With Rans-Cfd and Comparison With Full-Scale Ship Trials. *Brodogradnja*, 73(4), 107–129. https://doi.org/10.21278/brod73406

[9] Oltmann, P. Sharma, S. D., 1984. Simulation of Combined Engine and Rudder Maneuvers Using an Improved Model of Hull-Propeller-Rudder Interactions. in *Proc. of 15th Symposium on Naval Hydrodynamics*, Washington, DC, USA, 83–108.

[10] Dai, K., Li, Y., Gong, J., Fu, Z., Li, A., Zhang, D., 2022. Numerical Study on Propulsive Factors in Regular Head and Oblique Waves . *Brodogradnja*, 73(1), 37–56. https://doi.org/10.21278/brod73103

[11] Grlj, C., Degiuli, N., Farkas, A., Martić, I., 2023. Scale effects on self-propulsion characteristics of Japan Bulk Carrier. *10th International Conference on Computational Methods in Marine Engineering, MARINE 2023*, 27-29 June, Madrid, Spain. https://doi.org/10.23967/marine.2023.077

[12] Sano, M., 2023. Mathematical model and simulation of cooperative manoeuvres among a ship and tugboats . *Brodogradnja*, 74(2), 127–148. https://doi.org/10.21278/brod74207

[13] Dai, K., Li, Y., 2021. Experimental and numerical investigation on maneuvering performance of small waterplane area twin hull . *Brodogradnja*, 72(2), 93–114. https://doi.org/10.21278/brod72206

[14] Li, Y., Tang, Z., Gong, J., 2023. The effect of PID control scheme on the course-keeping of ship in oblique stern waves . *Brodogradnja*, 74(4), 155–178. https://doi.org/10.21278/brod74408

[15] Dlabač, T., Ćalasan, M., Krčum, M., Marvučić, N., 2019. PSO-based pid controller design for ship course-keeping autopilot. *Brodogradnja*, 70 (4), 1–15. https://doi.org/10.21278/brod70401

[16] Carrica, P.M., Castro, A.M., Stern, F., 2010. Self-propulsion computations using a speed controller and a discretized propeller with dynamic overset grids. *Journal of Marine Science and Technology*, 15(4), 316–330. https://doi.org/10.1007/s00773-010-0098-6

[17] Sezen, S., Dogrul, A., Delen, C., Bal, S., 2018. Investigation of self-propulsion of DARPA Suboff by RANS method . *Ocean Engineering*, 150, 258–271. https://doi.org/10.1016/j.oceaneng.2017.12.051

[18] Lungu, A., 2020. Numerical Simulation of the Resistance and Self-Propulsion Model Tests. *Journal of Offshore Mechanics and Arctic Engineering,* 142(2). https://doi.org/10.1115/1.4045332

[19] Kinaci, O.K., Gokce, M.K., Alkan, A.D., Kukner, A., 2018. On Self-Propulsion Assessment of Marine Vehicles . *Brodogradnja*, 69(4), 29–51. https://doi.org/10.21278/brod69403

[20] Kinaci, O.K., Gokce, M.K., Delen, C., 2020. Resistance experiments and self-propulsion estimations of Duisburg Test Case at 1/100 scale. *Ship Technology Research*, 67(2), 109–120. https://doi.org/10.1080/09377255.2020.1729454

[21] Delen, C., Can, U., Bal, S., 2020. Prediction of Resistance and Self-Propulsion Characteristics of a Full-Scale Naval Ship by CFD-Based GEOSIM Method. *Journal of Ship Research*, 234(4) 1–16. https://doi.org/10.5957/JOSR.03200022

[22] ITTC, 2014. 7.5-03-02-03 Recommended Procedures and Guidelines - Practical Guidelines for Ship CFD Applications.

[23] Siemens, 2019. Star-CCM+ User Guide version 14.02.

[24] Fureby, C., Anderson, B., Clarke, D., Erm, L., Henbest, S., Giacobello, M., Jones, D., Nguyen, M., Johansson, M., Jones, M., Kumar, C., Lee, S.K., Manovski, P., Norrison, D., Petterson, K., Seil, G., Woodyatt, B., Zhu, S., 2016. Experimental and numerical study of a generic conventional submarine at 10° yaw. *Ocean Engineering*, 116, 1–20. https://doi.org/10.1016/j.oceaneng.2016.01.001

[25] Zhang, L., Wei, Y., Deng, Y., Yin, H., Zhang, Y., Shang, Y., Zhang, J., 2021. A comparative investigation of fixed and free-running CFD self-propulsion models on a waterjet-propelled trimaran. *Ocean Engineering*, 232, 109081. https://doi.org/10.1016/j.oceaneng.2021.109081

[26] ITTC, 2011. 7.5-03-02-03 Recommended Procedures and Guidelines Practical Guidelines for Ship CFD Applications.

[27] Kim, D., Song, S., Tezdogan, T., 2021. Free running CFD simulations to investigate ship manoeuvrability in waves . *Ocean Engineering*, 236, 109567. https://doi.org/10.1016/j.oceaneng.2021.109567

[28] Feng, D., Yu, J., He, R., Zhang, Z., Wang, X., 2020. Free running computations of KCS with different propulsion models. *Ocean Engineering*, 214, 107563. https://doi.org/10.1016/j.oceaneng.2020.107563

[29] Aram, S., Mucha, P., 2023. Computational fluid dynamics analysis of different propeller models for a ship maneuvering in calm water. *Ocean Engineering*, 276. https://doi.org/10.1016/j.oceaneng.2023.114226

[30] Guo, C., Wang, X., Wang, C., Zhao, Q., Zhang, H., 2020. Research on calculation methods of ship model self-propulsion prediction. *Ocean Engineering*, 203, 107232. https://doi.org/10.1016/j.oceaneng.2020.107232

[31] Yu, J., Feng, D., Liu, L., Yao, C., Wang, X., 2022. Assessments of propulsion models for free running surface ship turning circle simulations. *Ocean Engineering*, 250. https://doi.org/10.1016/j.oceaneng.2022.110967

[32] Gokce, M.K., Kinaci, O.K., Alkan, A.D., 2019. Self-propulsion estimations for a bulk carrier. *Ships and Offshore Structures*, 14(7), 656–663. https://doi.org/10.1080/17445302.2018.1544108

[33] Dogrul, A., 2022. Numerical Prediction of Scale Effects on the Propulsion Performance of Joubert BB2 Submarine. *Brodogradnja*, 73(2), 17–42. https://doi.org/10.21278/brod73202

[34] ITTC, 2017. 7.5-02-02-03 Recommended Procedures and Guidelines - Resistance and Propulsion Test and Performance Prediction with Skin Frictional Drag Reduction Techniques.

[35] Liu, H.-L., Huang, T.T., 1998. Summary of DARPA Suboff Experimental Program Data. Report Number: CRDKNSWC/HD-1298-11. https://doi.org/10.21236/ADA359226

[36] ITTC, 2014. 7.5-02-02-02 Recommended Procedures and Guidelines – Resistance Uncertainty Analysis, Example for Resistance Test.

[37] Roache, P. J., 1997. Quantification of Uncertainty in Computational Fluid Dynamics. *Annual Reviews of Fluid Mechanics*, 29(1), 123–160. https://doi.org/10.1146/annurev.fluid.29.1.123

[38] Celik, I. B., Ghia, U., Roache, P. J., Freitas, C. J., Coleman, H., Raad, P. E., 2008. Procedure for estimation and reporting of uncertainty due to discretization in CFD applications. *Journal of Fluids Engineering, Transactions of the ASME*, 130(7), 0780011–0780014. https://doi.org/10.1115/1.2960953

[39] Chase, N., 2012. Simulations of the DARPA Suboff Submarine Including Self-propulsion with the E1619 Propeller. PhD Thesis, University of Iowa.